Tellus (2003), 55B, 837–854
Printed in UK. All rights reserved

TELLUS
ISSN 0280–6509

Effects of diapycnal and isopycnal mixing on the ventilation of CFCs in the North Atlantic in an isopycnic coordinate OGCM

By YONGQI GAO[1]*, HELGE DRANGE[1,2,3] and MATS BENTSEN[1,2], [1]*Nansen Environmental and Remote Sensing Center, Edv. Griegsv. 3A, N-5059 Bergen, Norway;* [2]*Bjerknes Centre for Climate Research, Bergen, Norway;* [3]*Geophysical Institute, University of Bergen, Norway*

(Manuscript received 17 July 2002; in final form 24 January 2003)

ABSTRACT

Simulated distributions of the chlorofluorocarbons CFC-11 and CFC-12 are used to examine the ventilation of the North Atlantic Ocean in a global version of the Miami Isopycnic Coordinate Ocean Model (MICOM). Three simulations are performed: one with a diapycnal diffusivity $K_d = 3 \times 10^{-7}/N$ m^2 s^{-1} and an isopycnal diffusive velocity (i.e., diffusivity divided by the size of the grid cell) $v_{trac} = 0.01$ m s^{-1} (Exp. 1); Exp. 2 is as Exp. 1 but with $K_d = 5 \times 10^{-8}/N$ m^2 s^{-1} plus increased bottom mixing; and Exp. 3 is as Exp. 2 but with $v_{trac} = 0.0025$ m s^{-1}. The main features of the simulated ventilation are strong uptake of the CFCs in the Labrador, Irminger and Nordic Seas, and a topographically aligned geostrophically controlled southward transport of CFC-enriched water in the Atlantic. It is found that the Overflow Waters (OW) from the Nordic Seas, the penetration of the western boundary currents, the ventilation of the subtropical surface waters, the vertical density stratification and the meridional overturning are all critically dependent on the applied isopycnal and diapycnal diffusivities, with Exp. 3 (Exp. 1) yielding the most (least) realistic results. Furthermore, it is the combined rather than the isolated effect of the isopycnal and diapycnal diffusivities that matter. For instance, the strength of the simulated Meridional Overturning Circulation (MOC) is similar in Exps. 1 and 3, but the simulated CFC-distributions are far too diffusive in Exp. 1 and fairly realistic in Exp. 3. It is demonstrated that the simulated distributions of transient tracers like the CFCs can be used to set the strength of the applied isopycnal mixing parameterization, a task that is difficult to conduct based on the simulated hydrography alone.

1. Introduction

The North Atlantic thermohaline circulation is an active and important component of the climate system, particularly on multi-annual to decadal timescales (e.g., Curry and McCartney, 2001; Eden and Jung, 2001). The warm and saline surface water flowing northward with the North Atlantic Current (NAC), the extension of the Gulf Stream current system further south in the Atlantic, transports large amounts of heat and salt poleward. A large part of the heat is released to the atmosphere, especially during the cold and windy winter months, contributing to the anomalous (high) temperatures of especially the northwestern Europe (e.g., Hartman, 1994; Rahmstorf and Ganopolski, 1999). Likewise, the transport of salt is crucial for the formation of dense surface waters in the Labrador and the Nordic Seas (here defined as the Greenland, Norwegian and Iceland Seas) (Furevik et al., 2002).

The dense water masses formed in the open ocean, together with dense brine water formed on the Arctic shelves during formation of ice (Jones et al., 1995; Rudels et al., 1994) form intermediate, and in some occasions, truly abyss water. The major branches of

*Corresponding author.
e-mail: yong@nersc.no

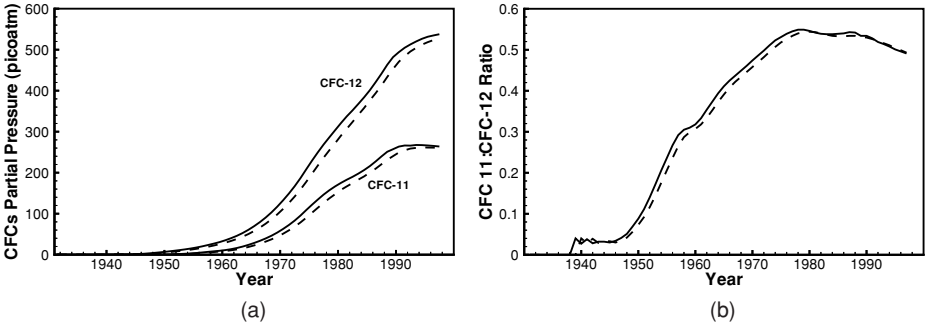

Fig. 1. (a) Reconstructed history of CFC-11 and CFC-12 partial pressure in dry air at one atmosphere pressure (Walker et al., 2000) and (b) ratio of CFC-11/CFC-12. The solid (dashed) line corresponds to the CFC concentrations and the CFC-11/CFC-12 ratio in the northern (southern) hemisphere.

the cold and dense intermediate to deep currents of the North Atlantic Ocean are known as the Deep Western Boundary Currents (DWBCs; Warren, 1981), and they form the lower limb of the thermohaline circulation (THC) cell (Gordon, 1986).

Climatological proxy data and numerical simulations indicate that the intensity of the thermohaline circulation is sensitive to the actual state of the climate system, and vice versa (Manabe and Stouffer, 1999). Therefore, reliable realizations of the past, present and future climate system, including regional climate predictions for various climate scenarios and, for instance, assessments of possible changes in the global ocean uptake of heat and the greenhouse gas CO_2, require a realistic representation of this circulation cell.

The chlorofluorocarbon trace gases CCl_3F (CFC-11) and CCl_2F_2 (CFC-12) were introduced to the atmosphere in the early 1930s. The atmospheric evolution of the CFCs have been monitored continuously since then (Fig. 1), and the oceanic concentration has been measured at several occasions and locations over the last 20 yr (see below). CFCs have no natural sources and are chemically and biologically inactive in the ocean, so the CFCs are well suited tracers to shed light onto seasonal to decadal timescale processes in the ocean and on the representation of these processes in Ocean General Circulation Models (OGCMs). Therefore, the measured distributions of CFCs have been used to examine the degree of realism of OGCMs (Dixon et al., 1996; Dutay et al., 2002), and to infer sources and mixing pathways of water masses in the ocean (Smethie et al., 2000) and in the OGCMs (England and Holloway, 1998). In a recent paper, England and Maier-Reimer (2001) argue that OGCM simulation with CFCs is a cost-effective approach to evaluate the inter-decadal ocean ventilation.

Furthermore, analysis of the observed distribution of CFCs in the North Atlantic has been performed to reveal the pathway of the DWBCs and to quantify the speed and mixing of these currents (Andrie et al., 1999). Using CFC observations obtained in 1992, Smethie et al. (2000) were able to identify two prominent sub-surface CFC-11 maxima in the western North Atlantic along 24°N. Both cores were intensified to the west, extending into the ocean interior. The upper CFC-11 core was related to the water masses formed in the Labrador Sea, known as the Upper Labrador Sea Water (ULSW; Pickart et al., 1996), whereas the lower one originates from the OW (Hansen and Østerhus, 2000) from the Nordic Seas.

In this paper, the CFC-11 burden on the North Atlantic Ocean water masses is simulated using a truly global version of MICOM (Bleck et al., 1992), coupled to a dynamic–thermodynamic sea ice model. Guided by earlier studies performed with a semi-global version of a similar model (Dutay et al., 2002), special attention has been paid to the representation of the timing, location, strength, advective transport and dispersive mixing of the ventilated water masses, and the oceanic responses to the strength of the diapycnal and ispycnal mixing parameterizations. This is, to our knowledge, the first numerical sensitivity experiment using CFCs in an isopycnic coordinate OGCM.

For the CFC experiments presented here, the choice of an isopycnic coordinate OGCM is appealing for mainly two reasons: the preferred plane of advective flow in the ocean is along, rather than across, planes of constant density, and the mixing is orders of magnitude weaker in the diapycnal than in the isopycnal direction

(Ledwell and Watson, 1993; Toole et al., 1994). These features are embedded into the isopycnic concept per se. In fact, in the absence of diapycnic mixing, the isopycnic interfaces can be viewed as material surfaces as there are no numerical mixing across these interfaces.

The paper is organized as follows: In section 2 we present a brief description of the model used in the experiments. In section 3 modelled results are shown and comparison are made with CFC-11, CFC-12 and hydrographic observations. The simulated CFC distributions are discussed and summarized in section 4.

2. Model description

As already stated, a global version of MICOM has been used in this study. In the horizontal, a local orthogonal grid system with one pole over Siberia and one pole over Antarctica was adopted (Bentsen et al., 1999). The horizontal grid scale is shown in Fig. 2 and varies between 50 and 200 km. Along the Equator, a local grid refinement is applied in a 10° latitudinal band. There are 24 layers in the vertical, of which the uppermost mixed layer (ML) has a spatial and temporal varying density. The specified potential densities of the sub-surface layers were chosen to ensure proper representation of the major water masses in the North Atlantic/Nordic Sea regions. The densities of the isopycnic layers (in σ_0-units) are 24.12, 24.70, 25.28, 25.77, 26.18, 26.52, 26.80, 27.03, 27.22, 27.38, 27.52, 27.63, 27.71, 27.77, 27.82, 27.86, 27.90, 27.94, 27.98, 28.01, 28.04, 28.07 and 28.10. The vertically homogeneous ML utilizes the Gaspar (1988) bulk parameterization for the dissipation of turbulent kinetic energy, and has temperature, salinity and layer thickness as the prognostic variables. In the isopycnic layers below, temperature and layer thickness are the prognostic variables, whereas salinity is diagnostically determined using the simplified equation of state by Friedrich and Levitus (1972). The bathymetry is computed based on the arithmetic mean of the ETOPO-5 data set (from National Geophysical Data Center, USA). No smoothing or adjustment of the topography were made.

The model is forced with monthly mean values of the NCAR/NCEP reanalysis (Kalnay et al., 1996) wind stress, short wave, long wave, latent and sensible heat fluxes, precipitation and sea level pressure fields by applying the Fairall et al. (1996) bulk parameterization for the momentum, heat and fresh water fluxes (Bentsen and Drange, 2000). The ML temperature and salinity are relaxed towards the monthly mean climatological values of Levitus and Boyer (1994) and Levitus et al. (1994), with a relaxation timescale of 30 d for a 50 m thick ML. The relaxation is reduced linearly with ML thickness exceeding 50 m, and it is set to zero in waters where sea ice is present in March (September) in the Arctic (Antarctic) to avoid relaxation towards temperature or salinity outliers in the poorly sampled polar waters.

The thermodynamic module incorporates freezing and melting of sea ice and snow-covered sea ice (Drange and Simonsen, 1996). The dynamic part of the sea ice module is based on the viscous-plastic rheology of Hibler (1979), where sea ice is considered as a two-dimensional contiunum. The dynamic ice module

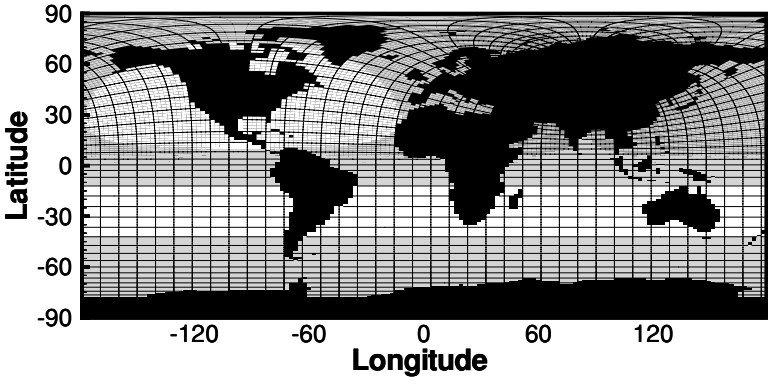

Fig. 2. The horizontal grid layout (every forth grid line is shown) and grid size (km) in the experiments. Grid size smaller than 150 km is shaded.

has been further modified by Harder (1996) to include description of sea ice roughness and the age of sea ice, and utilizing the advection scheme of Smolarkiewicz (1984).

The continuity, momentum and tracer equations are discretized on a C-grid stencil of Arakawa and Lamb (1977). The diffusive velocities (diffusivities divided by the size of the grid cell) for layer interface diffusion and momentum dissipation are 0.01 and 0.02 m s^{-1}, respectively, yielding actual diffusivities of about 10^3 m^2 s^{-1}. For the base-line integration (hereafter Exp. 1), the diffusive velocity for tracer (i.e., for temperature, salinity and the CFCs) dispersion $v_{\text{trac}} =$ 0.01 m s^{-1}. The flux corrected transport scheme by Smolarkiewicz and Clark (1986) is used to advect the model layer thickness and the tracer quantities. The processes governing the vertical mass transfer are described in section 2.1. Readers interested in the intrinsic details about MICOM are referred to Bleck et al. (1992).

2.1. Vertical mass transfer in MICOM

The seasonal cycle of the ML thickness in MICOM is governed by entrainment, detrainment and convection. When the turbulent kinetic energy is positive, i.e., when the generation of turbulence caused by wind stress or negative buoyancy forcing (caused by cooling or increased salinity of the ML) dominates over the positive buoyancy forcing and dissipation, entrainment occurs. The opposite situation holds for detrainment.

Convective mixing takes place if the density of the surface ML exceeds the density of one or more of the underlying isopycnals. The instability is removed by mixing all of the unstable water masses with the ML water, and by absorbing the new water mass into the ML. Both momentum and tracers (temperature, salinity and the CFCs) are instantaneously and uniformly mixed during convective adjustment episodes.

The interior layers exchange their properties with the ML if they outcrop to the base of the ML. Therefore, the location and timing of the outcropping layers are of central importance in analyzing the ocean ventilation of any of the ML properties.

The interior isopycnic layers which usually do not have direct contact with the atmosphere are considered to behave adiabatically, except for a density stratification dependent diapycnal mixing between the layers. For the base-line version of the model (Exp. 1), the diapycnal mixing coefficient K_{d} (m^2 s^{-1}) is parameterized according to the expression (Gargett, 1984)

$$K_{\text{d}} = \frac{3 \times 10^{-7}}{N}, \tag{1}$$

where

$$N = \sqrt{\frac{g}{\rho}\frac{\partial \rho}{\partial z}} (\text{s}^{-1})$$

is the Brunt–Väisälä frequency, g (m s^{-2}) is the gravity acceleration, ρ (kg m^{-3}) is the density and z (m) is the depth. The numerical implementation of eq. (1) follows the scheme of McDougall and Dewar (1998).

2.2. Sensitivity experiments

To examine the model sensitivity to the value of the diapycnal mixing K_{d}, a twin integration (hereafter Exp. 2) was performed in which $K_{\text{d}} = 5 \times 10^{-8}/N$ (m^2 s^{-1}), or a factor 6 below the value used in Exp. 1. To further account for increased mixing towards the sea floor (Munk and Wunsch, 1998; Ledwell et al., 2000), K_{d} in Exp. 2 was increased by a factor of four in the layers located within 100 m from the sea floor. The diagnosed diffusivities in the North Atlantic are illustrated in Fig. 3, together with a global estimate

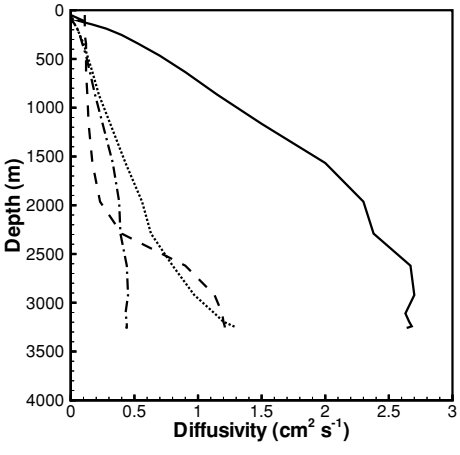

Fig. 3. Diagnosed diffusivity (cm^2 s^{-1}) in Exp. 1 (solid line), Exp. 2 (dotted line) and Exp. 2 but without enhanced bottom mixing (dash-dotted line). For comparison, the parameterization adopted for the global ocean by Hasumi and Suginohara (1999) is also displayed (long dashed line).

of K_d based on the study of Hasumi and Suginohara (1999).

A second twin integration was performed based on Exp. 2 by reducing the diffusive velocity for tracer dispersion v_{trac} by a factor of four (hereafter Exp. 3). The three experiments, forming two twin experiments, are therefore characterized by the following:

Exp. 1: $K_d = 3 \times 10^{-7}/N$ m^2 s^{-1}; $v_{trac} = 0.01$ m s^{-1},
Exp. 2: $K_d = 5 \times 10^{-8}/N$ m^2 s^{-1} plus increased bottom mixing; $v_{trac} = 0.01$ m s^{-1}, and
Exp. 3: $K_d = 5 \times 10^{-8}/N$ m^2 s^{-1} plus increased bottom mixing; $v_{trac} = 0.0025$ m s^{-1}.

2.3. Spin-up of the physical model

All of the three model simulations were initialized by the January Levitus and Boyer (1994) and Levitus et al. (1994) climatological temperature and salinity fields, respectively, a 2 m thick sea ice cover based on climatological sea ice extent (Gloersen et al., 1992), and an ocean at rest. The three experiments were then integrated in parallel for 110 yr by applying the monthly mean NCAR/NCEP atmospheric forcing fields, and temperature and salinity relaxation, as described above.

A spin-up integration of $\mathcal{O}$(100 yr) is far from sufficient to reach an annually steady state circulation of the deepest waters in the World Ocean, but is sufficient for the upper and intermediate waters, including the rapidly ventilated deep waters of the North Atlantic Ocean.

2.4. Set-up of the CFCs simulation

Following the atmospheric record (Fig. 1), the CFCs simulations begin in 1931 with zero concentrations in the atmosphere and the ocean. All experiments were run to the end of 1997.

The flux F (mol m^{-2} s^{-1}) of the CFCs at the air–sea surface are expressed as:

$$F = K_w(C_{sat} - C_{surf}) \quad (2)$$

where C_{sat} (mol m^{-3}) is the saturated CFCs concentration in moist air near the sea surface, K_w (m s^{-1}) is the transfer (or piston) velocity, and C_{surf} (mol m^{-3}) is the modelled surface ocean CFCs concentration. The transfer velocity K_w is computed using eq. (3) in Wanninkhof (1992). Further details are given by Dutay et al. (2002).

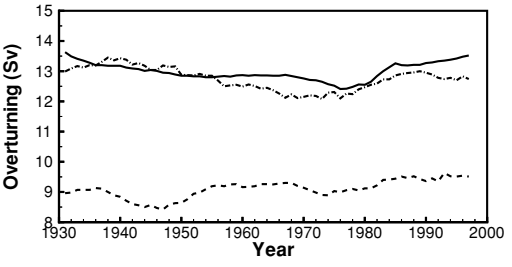

Fig. 4. Temporal variation of maximum overturning (Sv = 10^6 m^3 s^{-1}) along 24°N in the North Atlantic. The mean value for Exp. 1 (solid line), Exp. 2 (dotted line) and Exp. 3 (dash-dotted line) are 13.0, 9.1 and 12.8 Sv, respectively.

3. Results

3.1. Meridional overturning and zonal distribution of CFC-11

As already mentioned, the CFCs are passive tracers that are redistributed by advective transport and dispersive mixing along the isopycnals, and by mixing across the isopycnals. The simulated meridional overturning circulation (MOC), illustrating the major features of the meridional thermohaline circulation cell, is useful in displaying the modelled CFCs distribution.

Figure 4 shows the temporal evolution of maximum overturning at 24°N in the North Atlantic during the CFC simulations. The maximum overturning is fairly stable during the integrations. The maximum overturning occurs on the 27.52-isopycnal in Exps. 1 and 2, and on the 27.63-isopycnal in Exp. 3 (cf. Fig. 5 and discussion below), implying that the net southward flow of water masses occur with $\sigma_0 > 27.52$ in Exps. 1 and 2, and 27.63 in Exp. 3. The average overturning rates are 13.0, 9.1 and 12.8 Sv in Exps. 1, 2 and 3, respectively. The difference in the overturning rates illustrate the dependency on the strength of the diapycnal (e.g., Bryan, 1987; Sun and Bleck, 2001), as well as on the strength of the isopycnal (e.g., Schmittner and Weaver, 2001), mixing.

The simulated annual mean structure of the overturning in the Atlantic Ocean in Exps. 1 and 3 are displayed in Fig. 5. The zonally averaged concentration of CFC-11 in year 1990 and the maximum ML thickness are also shown in the figure. The MOC and zonally averaged concentration of CFC-11 are provided in both σ_0 and fixed depth (or z) coordinates, the latter by applying a vertical interpolation of the isopycnals with a vertical resolution of 20 m. Overall,

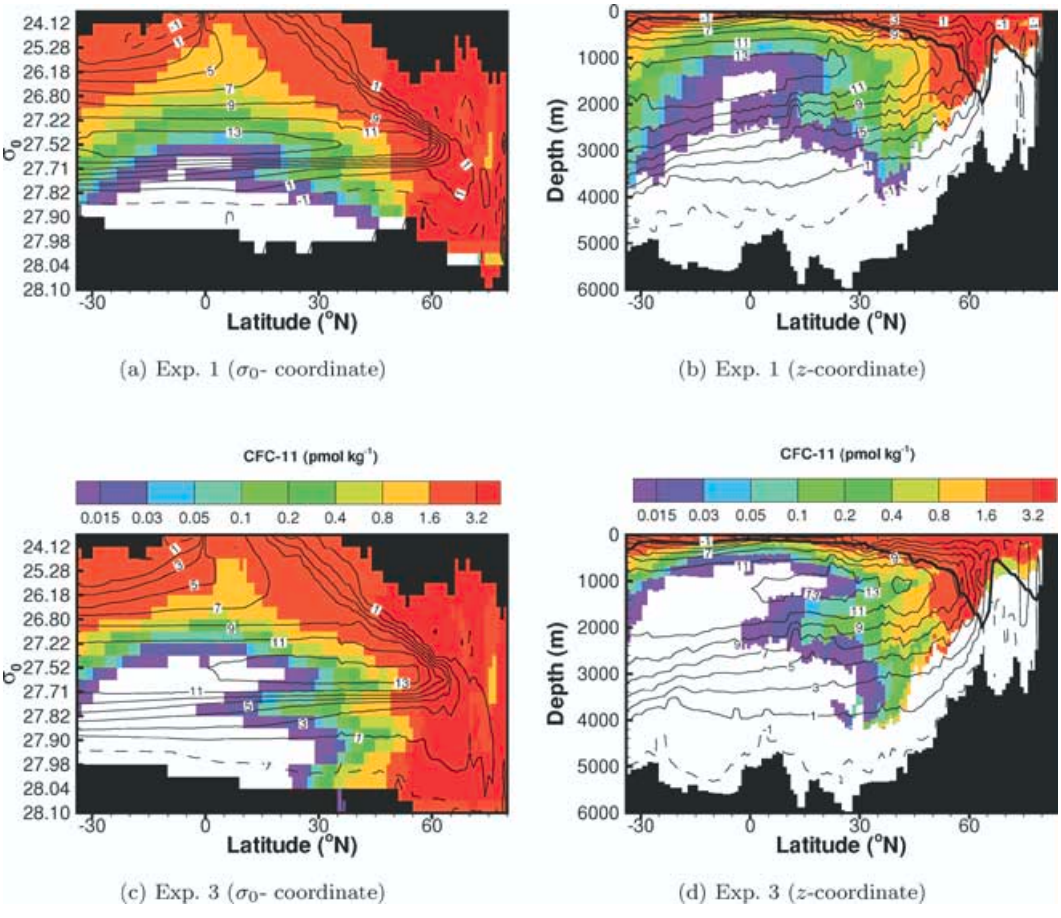

(a) Exp. 1 (σ_0- coordinate)

(b) Exp. 1 (z-coordinate)

(c) Exp. 3 (σ_0- coordinate)

(d) Exp. 3 (z-coordinate)

Fig. 5. Zonally averaged CFC-11 concentration in the Atlantic Ocean in 1990 (units pmol kg^{-1}, cut-off value 0.005 pmol kg^{-1}) from Exp. 1 (upper panels) and Exp. 3 (lower panels). The left panels show the CFC-11 concentration and overturning (2 Sv isolines) as function of potential density and latitude. The right panels show the same quantities as function of depth and latitude. Solid (dashed) lines indicate clockwise (counter-clockwise) circulation looking west, and the thick lines in the right panels indicate the maximum ML thickness in the model. The black areas in the σ_0-panels correspond to water masses that are absent at the given latitude.

both experiments capture the so-called Global Conveyor Belt (GCB; Broecker, 1991) circulation. At the surface, the warm and light water becomes denser as it moves poleward. At high northern latitudes, the dense surface water sinks and flows southward at intermediate to abyssal depths to close the thermohaline circulation cell.

Highest CFC-11 concentrations occur at the surface at the high latitudes mainly because of the wind and buoyancy generated mixing and temperature dependency on the solubility of the CFCs. Deep penetration of CFC-11 therefore occurs where deep surface mixing and winter time convection are present with subsequent subduction of the ventilated waters (McCartney and Talley, 1982; New et al., 1995). The shallow penetration of CFC-11 near the Equator is mainly due to the strong thermocline (implying weak diapycnal mixing), and consequently shallow ML there. The southward flow of dense water in the North Atlantic Ocean dominates the lower parts of the GCB, illustrating the unique properties of these water masses.

The outflow of NADW with enhanced CFC-11 concentration at intermediate depths is captured in both experiments (panels 5b and 5d) at about 2000 m.

Moreover, a deep outflow of NADW with a high CFC-11 signal is captured in Exp. 3 (and to some extent in Exp. 2, not shown) at a depth of about 4000 m. Figures 5a and 5c confirm that the southward moving deep water masses have potential density > 27.52 in Exp. 1 (and Exp. 2, not shown) and >27.63 in Exp. 3.

In Exp. 1 the outflow of NADW is about 13 Sv in the subtropical North Atlantic (Figs. 5a and 5b), which is in accordance with the estimated value of 13 ± 2 Sv according to Ganachaud and Wunsch (2000) within the similar density range. The transport of NADW across Equator is also about 13 Sv, which is consistent with the estimate of 14 Sv by Schmitz (1995), and is in the range 12–15 Sv estimated by Dickson and Brown (1994). In the sub-surface waters, the most southward-reaching water mass tagged with CFC-11 has a potential density between 27.71 and 27.77 (Fig. 5a), and the zonal average depth of this CFC-11 tongue is 2000–2600 m at the Equator (Fig. 5b). It is seen that the sub-surface CFC-11 tongue originating from the North Atlantic has passed the Equator in 1990, which implies an efficient ventilation and spreading of the corresponding water mass. Furthermore, the northward concentration gradient of the CFC-11 tongue indicates that the source of the ventilation of this water mass originates north of 50°N.

The overturning features of Exps. 2 (not shown) and 3 differ from those of Exp. 1 by the following: a deep CFC-11 tongue located at about 4000 m is present in Exps. 2 and 3, but not in Exp. 1. This finding is further addressed in section 3.6. Maximum overturning is weak in Exp. 2, but consistent with Exp. 1 (and with observational based estimates) in Exp. 3. In addition, the southward extension of the CFC-enriched water masses at depths of 2000–2500 m is less profound in Exps. 2 and 3 compared to that in Exp. 1.

To further elucidate on the relationship between the CFC-enriched water masses and the overturning, the mass transport of each isopycnic layer and the overturning across 24°N in the North Atlantic for CFC year 1990 are depicted in Fig. 6 (the corresponding transports for the other years are very similar).

In Exp. 1 (Fig. 6a) the major part of the water masses with density less than 27.52 flow northward, and the water masses with $\sigma_0 > 27.52$ flow southward. As already mentioned, the water mass 27.71 dominates the transport of the southward-flowing waters. The transport rate of this water mass reaches 9.1 Sv, and contributes about 67% of the total southward mass transport across 24°N. The dominant transport rate of the 27.71-isopycnal is the reason for the prominent southward-reaching tongue of CFC-11 in Exp. 1. The value of the overturning at the bottom is about 1.2 Sv. This transport originates from the flow through the Bering Strait, and is close to the observational based estimate of 1 Sv (Roach et al., 1995).

For Exps. 2 (not shown) and 3, the transports are generally weaker than those in Exp. 1. There are two exceptions to this: The ML transport in Exps. 2 and 3 exceeds the transport in Exp. 1 by a factor two to three, and a second sub-surface maximum occurs on the 27.90-isopycnal.

3.2. *The high-latitude winter mixing*

After examining at the meridional penetration of CFC-11, attention is turned to the location of the deep mixing in the North Atlantic, and the water

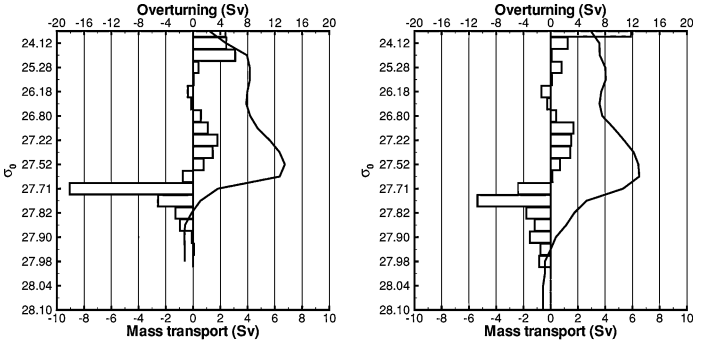

(a) Exp. 1 (b) Exp. 3

Fig. 6. The mass transport (Sv; bars) on each isopycnal and the overturning (Sv; solid line) across 24°N in the North Atlantic from CFC-year 1990: (a) from Exp. 1, and (b) from Exp. 3. Positive (negative) values indicate northward (southward) transports.

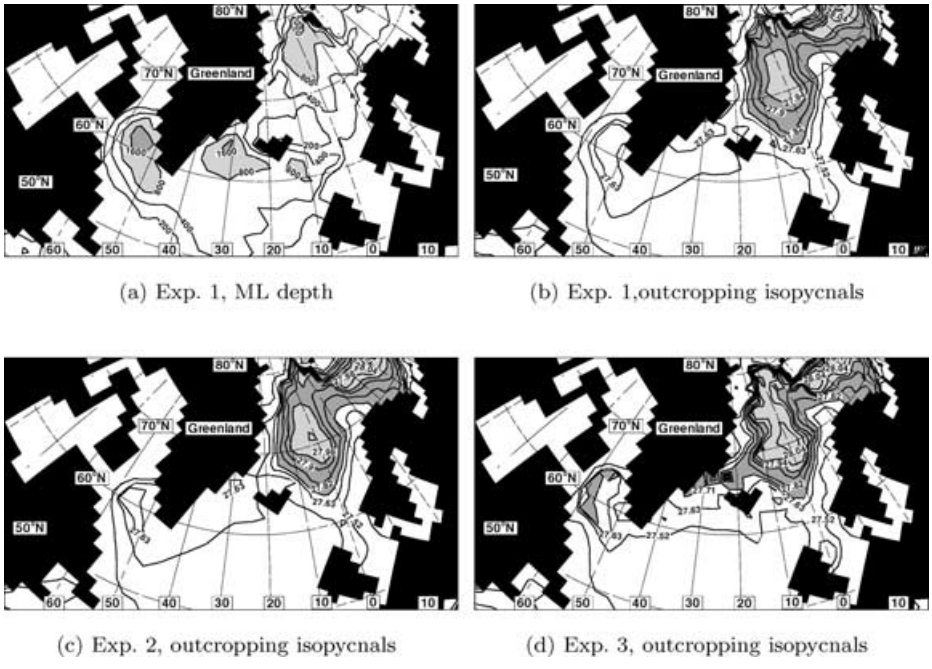

(a) Exp. 1, ML depth (b) Exp. 1,outcropping isopycnals

(c) Exp. 2, outcropping isopycnals (d) Exp. 3, outcropping isopycnals

Fig. 7. Simulated ML thickness (m) (a) and location of the outcropping isopycnals (b) in April 1990 of Exp. 1. (c) and (d) are as (b) but for Exps. 2 and 3, respectively. ML thickness exceeding 800 m and potential densities >27.71 are shaded.

masses that are ventilated with the ML during winter. Figure 7 shows the ML thickness in April 1990 in Exp. 1, and the locations of the outcropping isopycnals in the northern North Atlantic and in the Nordic Seas for all of the experiments.

Deep convective mixing reaches a depth of 1600–2000 m in the Labrador and Irminger Seas, and here the 27.63-isopycnal outcrops to the surface. Therefore, a strong CFC-11 signal is expected on the 27.63-isopycnal (or at a depth of 1600–2000 m). Similarly, the simulated convective mixing reaches a depth of 800 m in the Greenland Sea and here the 27.94-isopycnal outcrops to the surface. As a result, strong CFC-11 signals originating from the Nordic Seas are expected on the isopycnals with potential densities greater than those of the simulated Labrador Sea Water (LSW).

The simulated ML depth of Exps. 2 and 3 are close to that of Exp. 1 (not shown). The otcropping region of the isopycnals in Exps. 2 and 3 are also similar to those of Exp. 1 (Figs. 7c and 7d). However, compared to Exp. 1, the densities of the outcropping layers are slightly higher in Exp. 2 and, for the Nordic Seas, significantly higher in Exp. 3. The difference in the vertical density structure in the Nordic Seas among the three experiments has important implications for the simulated OW characteristics as discussed in section 3.6.

3.3. Ventilation of the thermocline

The panels in Fig. 8 show the observed and simulated concentrations of CFC-11 and the vertical position of the 27.52 and 27.77 isopycnals along the Tropical Atlantic Study (TAS), Leg 2 (Weiss et al., 1985). For Exp. 3, the simulated distributions of CFC-11 in the upper waters resemble the observation closely, whereas Exp. 1 is clearly too diffusive. It is also seen that, even after a total integration time of 162 yr, the position of the 27.52 isopycnal in Exp. 3 is almost indistinguishable from the climatological mean position (the latter based on Levitus and Boyer, 1994; Levitus et al., 1994). For comparison, the 27.52 isopycnal has descended by almost 100 m in Exps. 1 and 2.

Based on the simulated vertical density stratification, the strength of the applied diapycnal diffusivity in the upper water column is about 0.16×10^{-4} m^2 s^{-1} in Exp. 3, or within the estimated value of (0.11–0.17) $\times 10^{-4}$ m^2 s^{-1} based on a purposefully tracer release experiment in the thermocline of the subtropical

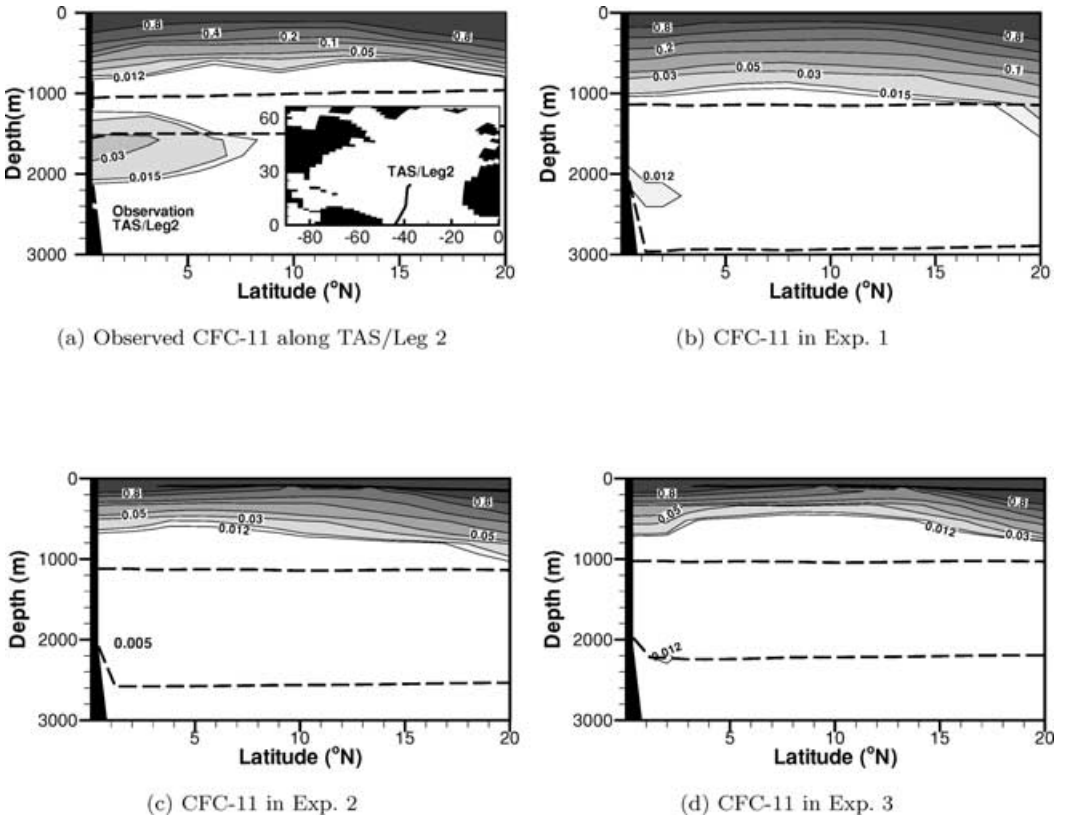

(a) Observed CFC-11 along TAS/Leg 2

(b) CFC-11 in Exp. 1

(c) CFC-11 in Exp. 2

(d) CFC-11 in Exp. 3

Fig. 8. Observed (a) and simulated (b–d) CFC-11 concentrations (pmol kg^{-1}) along TAS/Leg 2 (inlet in panel a) in early 1983 (Weiss et al., 1985). The cut-off value is 0.01 pmol kg^{-1}, with the indicated 0.005 pmol kg^{-1} as concentration of the sub-surface maximum in Exp. 2 (panel c). The long dashed lines show the position of the 27.52 and 27.77 isopycnals.

Atlantic Ocean (Ledwell and Watson, 1993; Ledwell et al., 1998), and also similar to the value adopted by Hasumi and Suginohara (1999) (see Fig. 3). In Exp. 1, the diagnosed diffusivity is about 1.5×10^{-4} $m^2\ s^{-1}$, or more than one order of magnitude above the cited Ledwell and Watson (1993) and Ledwell et al. (1998) values. The corresponding value for Exp. 2 is $0.2 \times 10^{-4}\ m^2\ s^{-1}$. Thus, the ventilation of the thermocline in the subtropical Atlantic is highly sensitive to the strength of the diapycnal mixing. Furthermore, the difference between Exps. 2 and 3 show that also the applied isopycnal mixing is of importance for the vertical distribution of the tracer (see below). For the applied model system, it follows that $K_d = 5 \times 10^{-8}/N\ m^2\ s^{-1}$ and $v_{trac} = 0.0025\ m\ s^{-1}$ yield a realistic ventilation rate of the thermocline waters in the sub-tropical Atlantic Ocean.

3.4. Ventilation of the sub-surface water masses

The Upper Labrador Sea Water (ULSW) is one component of the NADW (Bower and Hunt, 2000). The presence of recently formed and CFC-enriched ULSW in the Tropical Atlantic has been discussed, for instance, by Weiss et al. (1985) and Andrie et al. (1999). In the observation (Fig. 8a), the outflow of ULSW, which is believed to be formed in the Southern Labrador Sea (Pickart, 1992), is clearly present by the core with high CFC-11 concentration near 1700 m depth (Weiss et al., 1985) and with potential density of close to 27.77 (the latter calculated from Levitus and Boyer, 1994; Levitus et al., 1994).

The simulated CFC-11 distributions yield a sub-surface core of CFC-11, but there are apparent differences compared to the observation: For Exps. 1 and

2, the simulated cores have a potential density of 27.71 (or 0.06 σ_0 units below the observed density), whereas the density of the core of Exp. 3 matches the observation. For all of the experiments, the depths of the cores of CFC-enriched water are located at about 2200 m depth (or 600 m below the observation). In addition, the simulated CFC-11 concentrations are significantly underestimated.

The simulated stratification in the uppermost 1100 m ($\sigma_0 < 27.52$) is, as already described, quite close to the climatological density stratification. However, the stratification in the deeper waters ($\sigma_0 > 27.52$) has experienced a drift, which will be addressed in section 4. For instance, the location of the 27.77-isopycnal is at 1500 m in the climatology, 2900 m in Exp. 1, 2600 m in Exp. 2 and 2200 m in Exp. 3.

To illustrate the presence of both ULSW and OW using CFC-11, the observed and simulated CFC-11 along 24°N in the North Atlantic, together with the corresponding distribution of the 27.77 and 27.90 isopycnals, are displayed in Fig. 9. In the observation, two sub-surface maxima of CFC-11 are present, one at about 1500 m, the other between 3000 m and 4500 m. These sub-surface CFC-11 maxima correspond to the outflow of ULSW and OW, respectively (Smethie et al., 2000). The water mass corresponding to the shallow CFC-11 maximum has potential density of about 27.77 (cf. Fig. 8a), and the deep CFC-11 maximum has potential density > 27.86 (calculated from Levitus and Boyer, 1994; Levitus et al., 1994).

In Exp. 1, the model shows a CFC-11 maximum at the depth of 2000 m, but no deep core. The sub-surface maximum of CFC-11 corresponds to water with potential density of 27.71, which is the same as in the section along TAS/Leg 2 in Fig. 8b. An additional mismatch is present in the CFC-11 penetration depth in the Eastern North Atlantic Ocean (NEA), where the simulated CFC-11 signal penetrates far deeper than in the observation. The situation for Exp. 2 is close to that of Exp. 1, and is still far from the observed distribution.

A significant improvement is obtained in Exp. 3. Here a CFC maximum is found on the western part of the basin with potential density of 27.77. Apparently, the second sub-surface CFC maximum between 3000 m and 4500 m is not present in Exp. 3. However, OW does form the lower part of the simulated CFC-plume on the western side of the section. This is illustrated in Fig. 9f, displaying the CFC-11/CFC-12 ratio of the CFC-enriched water masses. Since the atmospheric CFC-11/CFC-12 ratio increases with time until the 1980s (Fig. 1b), the more recently ventilated water masses have a higher CFC-11/CFC-12 ratio than older water masses. It therefore follows from Fig. 9f that the lower part of the simulated CFC plume at a depth of about 4000 m and with density of 27.90 is more recently ventilated than the overlaying water masses. It is further shown in section 3.6 that the 27.90 water mass originates from the Nordic Seas. For comparison, the CFC-11/CFC-12 ratio of the CFC-enriched sub-surface water in Exp. 2 yield no indications of a secondary sub-surface CFC maximum at 24°N (Fig. 9e).

The vertical distribution of the simulated CFC-11/CFC-12 ratio near 70°W in Exp. 3, and consequently tof the ventilated water masses in the region of the DWBC at 24°N, is shown in Fig. 10. Clearly, the simulated CFC-11/CFC-12 ratio is too low for all of the sub-surface waters. However, the observed and simulated vertical CFC-11/CFC-12 distributions of the intermediate to deep waters are broadly consistent, including the presence of the secondary maximum near 4000 m. This is, to the best of our knowledge, the first successful CFC simulation producing the double DWBC core at 24°N.

Finally, it is shown in section 3.6 that the simulated CFC-enriched water in the eastern side of the basin in Exp. 3 (Fig. 8d) originates from the Nordic Seas as well. This finding is not in accordance with the observed CFC-11/CFC-12 ratio at 24°N (not shown), and this inconsistency is addressed in the section 4.

3.5. Spreading of the Labrador Sea water

Given that the simulated surface mixing in the subtropical North Atlantic can only reach the depth of several hundred metres (panels 5b and 5d), candidates for the presence of the excessive CFC-11 penetration in the NEA (and partly also in the NWA) are too strong isopycnic transport or mixing. To check this, the distribution of CFC-11 are examined on the ventilated isopycnals.

Figure 11 displays the observed and the simulated CFC-11 concentrations in early 1990 on the isopycnal in the centre of the upper DWBC core. The distribution of CFC-11 shows that the source water originates form the Labrador and Irminger Seas (and, caused by the lack of observations, possibly further upstream into the Nordic Seas) in the observations (Smethie et al., 2000), and in the Labrador, Irminger and Nordic Seas in the simulations. The simulated and observed concentrations of CFC-11 in the sub-polar source region are comparable and all simulations capture the

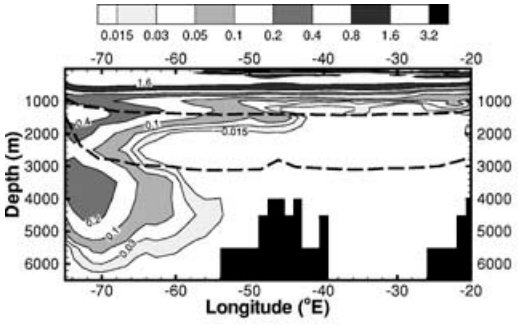

(a) Observed CFC-11 along 24°N in August, 1992

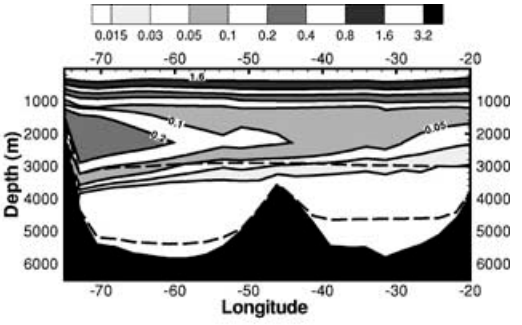

(b) CFC-11 in Exp. 1

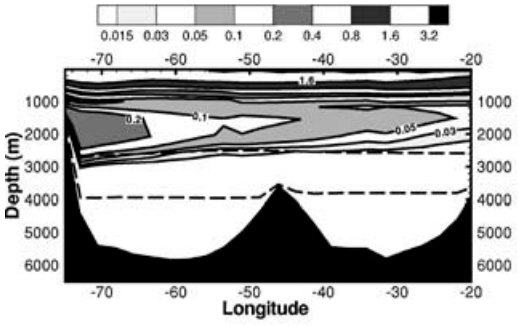

(c) CFC-11 in Exp. 2

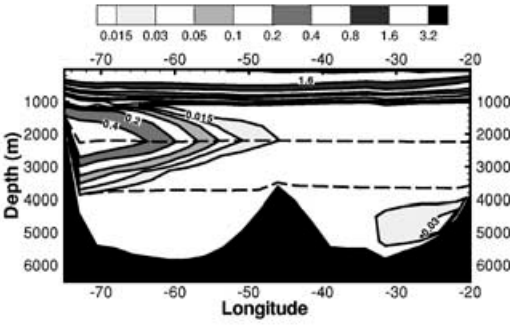

(d) CFC-11 in Exp. 3

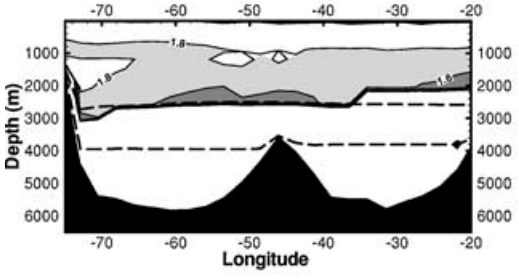

(e) CFC-11/CFC-12 in Exp. 2

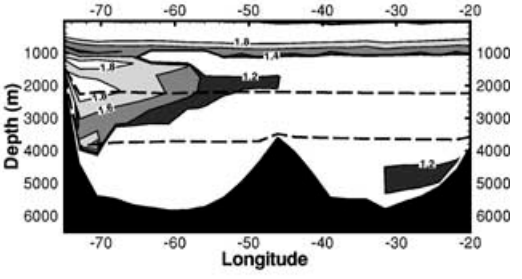

(f) CFC-11/CFC-12 in Exp. 3

Fig. 9. (a) Observed and (b–d) simulated CFC-11 concentration (in grey shading, unit pmol kg^{-1}, cut-off value 0.01 pmol kg^{-1}), and (e, f) the diagnosed CFC-11/CFC-12 ratio along WOCE Section A05 along 24°N in August 1992 (Bryden et al., 1996). The long dashed lines show the position of the 27.77 and 27.90 isopycnals.

observed southward transport of CFC-11. However, the observed spreading of CFC-11 along the western boundary is faster than simulated, in particular for Exp. 2.

In Exp. 1, the simulated equator-ward speed of ULSW in the Sub-tropical and Tropical Atlantic is less than 0.02 m s^{-1}, which is below the observed estimates of 0.02–0.04 m s^{-1} (Bower and Hunt, 2000).

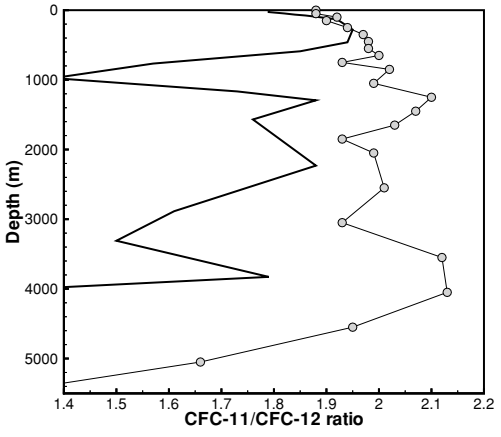

Fig. 10. The mean observed (circles) and simulated (line; Exp. 3) CFC-11/CFC-12 ratio between 70–72°W along WOCE Section A05 at 24°N in August 1992.

The simulated depth of the isopycnic interfaces is also displayed in the figure. This clearly shows that the CFC-11 core is located at a depth of 2200–2300 m in the Subtropical and Tropical Atlantic, as was shown in the vertical sections of the CFC-11 distribution (Fig. 8b).

In Exps. 2 and 3, the simulated equator-ward velocity at the ULSW level are <0.01 m s^{-1} and <0.02 m s^{-1}, respectively. Consequently, Exp. 2 has a simulated CFC-11 tongue that is even more sluggish than that of Exp. 1, whereas Exp. 3 gives the most realistic (but still underestimated) transport along the western boundary.

Figures 11b and 11c indicate that the reason for the deep presence of CFC-11 in the central and eastern North Atlantic at 24°N as seen in Figs. 9b and 9c is caused by isopycnal transport or mixing of the waters originating from the the high northern latitudes.

The apparent diffusive velocity $\boldsymbol{V}_{\text{diff}}$ (m s^{-1}) on an isopycnic layer can be diagnosed as (Smolarkiewicz, 1984)

$$\boldsymbol{V}_{\text{diff}} = \frac{K_{\text{iso}}}{hC}\nabla_{\text{iso}}(hC) \tag{3}$$

where K_{iso} (m^2 s^{-1}), ∇_{iso} (m^{-1}), h (m) and C (mol m^{-3}) are the diffusion coefficient, the isopycnic gradient operator, the layer thickness and the CFCs concentration on the actual isopycnal, respectively. The ratio between the advective and the apparent diffusive velocity on the 27.71-isopycnal in Exp. 1 is shown in Fig. 12. It is seen that the advective transport dominates in the OW regions and along the DWBC in the model, whereas the apparent diffusive transport is responsible for the spreading of the CFCs into the central and eastern North Atlantic Basin. The latter finding indicates that the applied isopycnal diffusive velocity of 0.01 m s^{-1} is too large by a factor two to five. This also explains why Exp. 3, with a horizontal diffusive velocity of one fourth compared to Exps. 1 and 2, greatly improves the simulated distribution of the sub-surface CFC-enriched water masses.

3.6. Spreading of the overflow water

Figure 13 shows the observed and simulated CFC-11 of the OW. In Exp. 1, the CFC-11 tongue reaches about 50°N, which is far less than in the observation. In addition, most of the OW remains in the NEA, contrary to the main observed pathway of these water masses. In fact, it is believed that most of the Iceland-Scotland Ridge (ISR) OW flows southward and parallel to the Reykjanes Ridge, crossing the North Atlantic Ridge at the Charlie–Gibbs Fracture Zone at 57 °N, and thereafter continues along the continental slope of the NWA as a part of the DWBCs.

In Exp. 2 the outflow of CFC-enriched OW reaches about 25°N, with the outflow through the Denmark Strait ventilating the NWA, and the outflow across the ISR ventilating the NEA.

Again Exp. 3 is closest to the observed distribution of the CFCs. Here the OW through the Denmark Strait, and partly also the OW across the ISR, flow southward in the NWA as the deep part of the DWBC. A significant fraction of the ISR OW is, however, still being found in the NWA.

4. Discussion and conclusion

To illuminate the decadal scale ventilation of the North Atlantic surface waters, and to perform a first-order assessment of the response of the ventilation to diapycnal and isopycnal mixing, the atmospheric tracers CFC-11 and CFC-12 have been embedded into a global version of the isopycnic coordinate ocean model MICOM.

Three model experiments have been performed: The base-line experiment (Exp. 1) is characterized by a diapycnal mixing coefficient $K_{\text{d}} = 3 \times 10^{-7}/N$ [m^2 s^{-1}; N (s^{-1}) is the Brunt–Väisälä frequency], and an isopycnal diffusion velocity $v_{\text{trac}} = 0.01$ m s^{-1}. Experiment 2 is identical to Exp. 1 but with

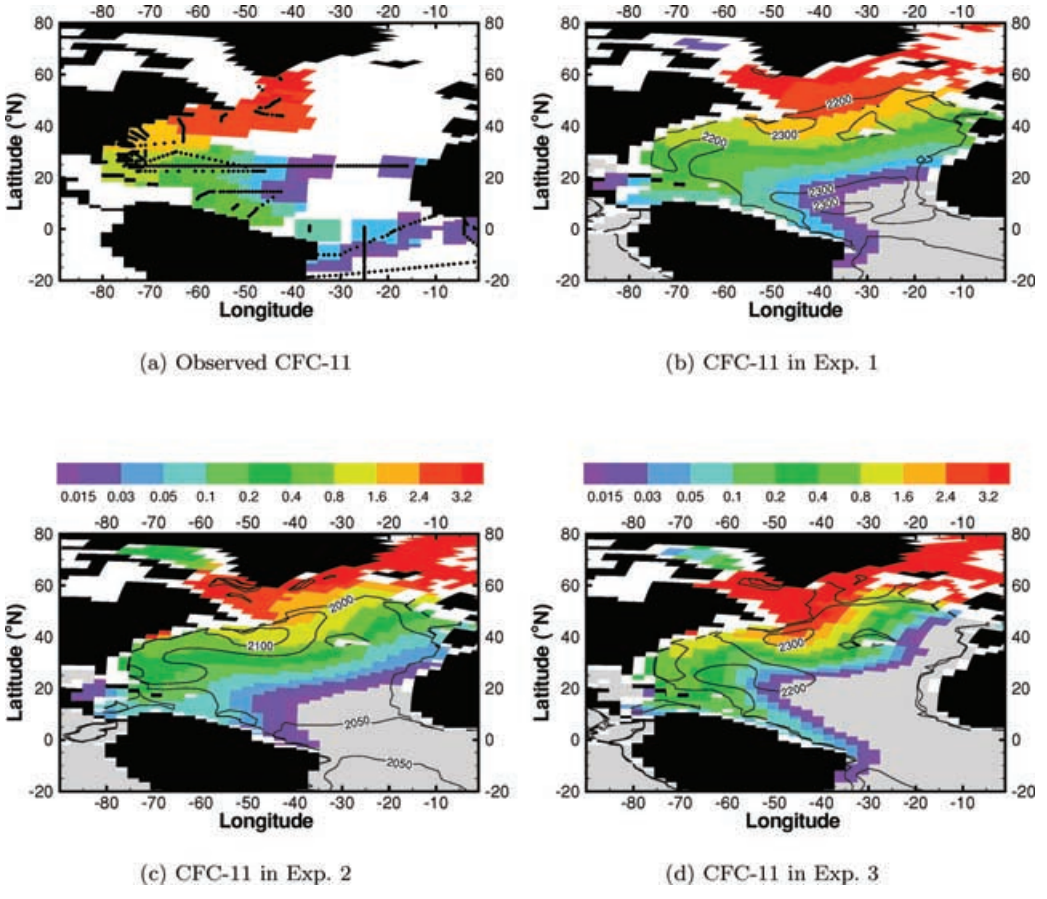

Fig. 11. CFC-11 concentration (pmol kg^{-1}, cut-off value 0.01 pmol kg^{-1}) in the outflow of UNADW in early 1990. In panel (a) observed CFC-11 (Smethie et al., 2000) is given with stations included as black dots. The black contour line denotes the depth of the isopycnal, grey color shows the presence of the simulated $\sigma_0 = 27.71$ water mass in Exps. 1 and 2, and $\sigma_0 = 27.77$ in Exp. 3.

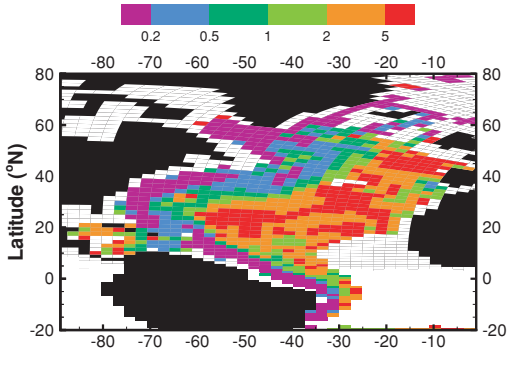

Fig. 12. Ratio of the apparent diffusive velocity to advective velocity on the 27.71-isopycnal in Exp. 1.

$K_d = 5 \times 10^{-8}/N$, plus enhanced mixing near the sea floor. Experiment 3 follows Exp. 2, but with $v_{trac} = 0.0025$ m s^{-1}. The three experiments, forming two twin experiments, show that the local to basin scale ocean dynamics and the associated transport and mixing of the CFCs are highly sensitive to the strength of the diapycnal and isopycnal mixing parameterizations.

It is demonstrated that it is generally needed to consider the combined, rather than the isolated, effect of the diapycnal and isopycnal mixing in validating OGCMs. For instance, adjustments of the diapycnal (or vertical) diffusion coefficient can be used to tune the simulated strength of the MOC. However, changes in the isopycnal (or horizontal) diffusion coefficient will also induce changes in the strength of the MOC

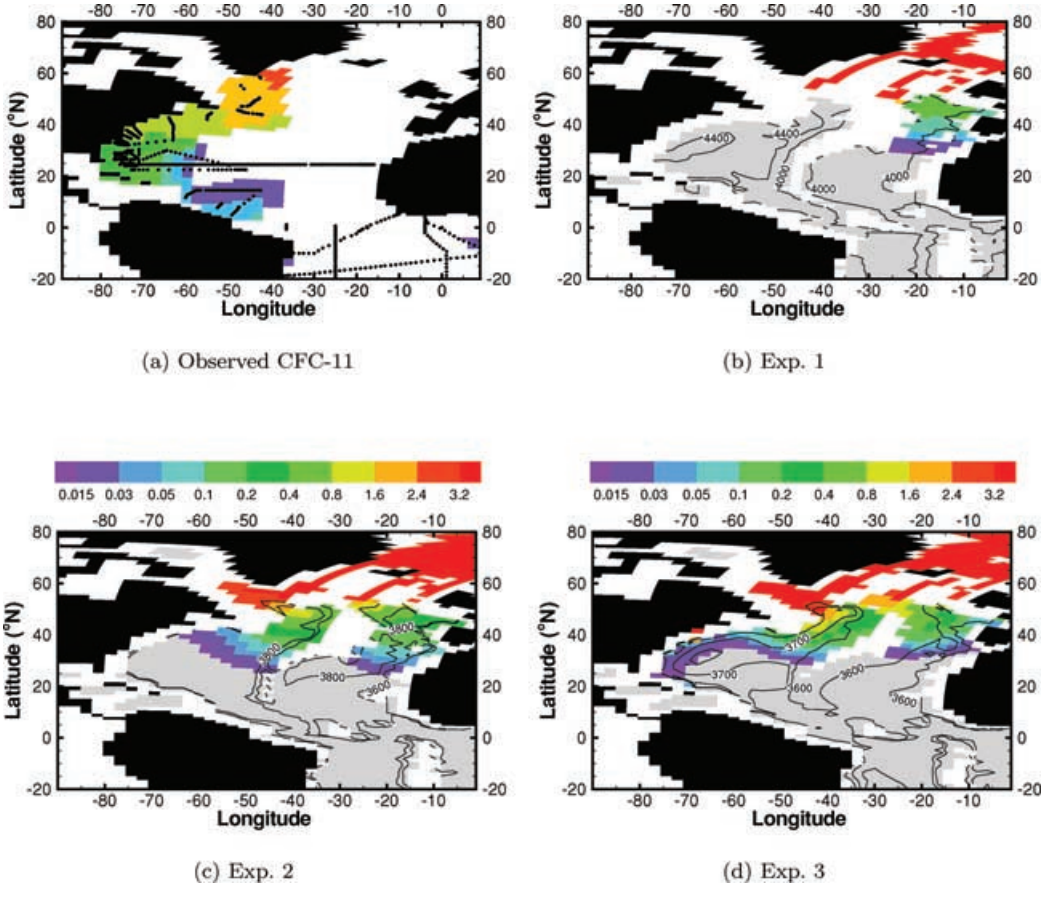

Fig. 13. As Fig. 11, but for the OW.

(cf. Fig. 4). It is therefore not known which combination of the diapycnal and isopycnal mixing coefficients (which both yield a fairly realistic MOC and a realistic ventilation of the surface and sub-surface water masses) occurs.

By introducing the CFCs as tracers to the model system, additional and powerful constraints are added to the model validation. From the present study, this is especially evident for the ventilation of the tropical thermocline (Figs. 8b, 8d, 9b and 9d), the spreading of the sub-polar and the less dense part of the OW (Fig. 11) and the OW forming the deep core of the DWBC (Fig. 13).

The conclusion from the present model exercise is that the experiment with both reduced diapycnal and isopycnal diffusivity (Exp. 3) is superior to the other model experiments for all of the CFC model-data comparisons that have been assessed. In addition, the depth of some of the key isopycnals that take part in the surface and sub-surface ventilation of the North Atlantic shows that Exp. 3 is closest to the observations (Table 1), and consequenlty the model version that

Table 1. *Comparison between observed (based on Levitus and Boyer, 1994; Levitus et al., 1994) and simulated (Exps. 1–3) mean depth (m) of the indicated isopycnals along the TAS/Leg 2 section in early 1983 (Fig. 8) and the WOCE Section A05 at 24°N in 1992 (Fig. 9)*

		Observed	Exp. 1	Exp. 2	Exp. 3
TAS/Leg 2	$\sigma_0 = 27.52$	1050	1140	1130	1030
	$\sigma_0 = 27.77$	1500	2925	2565	2220
A05, 24°N	$\sigma_0 = 27.77$	1411	3000	2600	2200
	$\sigma_0 = 27.90$	3095	4990	3850	3800

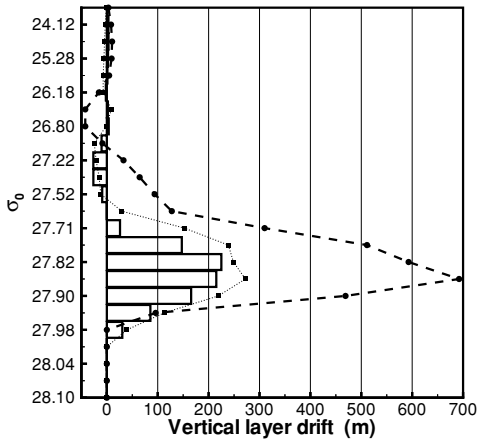

Fig. 14. Mean vertical layer drift (m) during the CFC integrations (i.e., the difference between CFC years 1992 and 1931) across the DWBC along A05 section at 24°N in the North Atlantic. Exp. 1, dased line; Exp. 2, dotted line; Exp. 3, bars.

experiences least model drift. The latter point is exemplified in Fig. 14, showing the vertical layer drift (positive values means deepening of the isopycnals) across the DWBC at 24 °N between CFC year 1992 and 1931. It follows that the layer drift is largest in Exp. 1 and smallest in Exp. 3.

The main differences between the simulated features of Exp. 3 and the observed CFCs are linked to too weak and sluggish DWBCs in the model. The problem with the deepest of the two DWBC plumes is partly caused by the part of the OW that flows across the ISR. It was demonstrated in section 3.6 that all of the model experiments show a tendency for the ISR OW to be confined to the NEA, whereas the major part of this water should cross the North Atlantic Ridge at the Charlie–Gibbs Fracture Zone at 57 °N. The reason for this model deficiency is connected to the vertical position of the isopycnals carrying the ISR OW. If the isopycnals with the ISR OW are located deeper than the North Atlantic Ridge in the model, the OW will necessarily be confined to the NEA. It follows from Fig. 9 and Table 1 that the vertical position of the 27.90 isopycnal is too deep in all experiments. The situation is clearly poorest for Exp. 1, whereas Exp. 3 is slightly improved compared to Exp. 2.

In the absence of formation of intermediate to deep waters and in the presence of diapycnal mixing, the OW will disappear with time, and the deepest isopycnals will descend in the water column. The OW isopycnals will also experience a net loss of mass and therefore descend in the water column if the diapycnal mixing flux exceeds the transport rate of the corresponding OW at the GSR. This is clearly the situation in Exp. 1; here the diapycnal mixing far exceeds the formation of the OW, leading to a quick conversion of dense to less dense water masses (e.g. Fig. 13b).

The 27.90 isopycnal in Exp. 3 is located sufficiently high in the water column (Fig. 9d) that part of the OW is able to cross the North Atlantic Ridge (Fig. 13d). However, a part of the OW in the NEA is not able to cross the ridge, leading to a sub-surface CFC maximum in the basin (Fig. 9d), and consequently to a reduced intensity of the deepest branch of the simulated DWBC (Fig. 13d).

A realistic representation of the DWBCs in OGCMs in general is further complicated by a usually coarse horizontal model resolution. This implies a model bathymetry that most likely do not properly resolve important topographic features as the Faroe-Bank Channel and the Charlie–Gibbs Fracture Zone. In addition, coarse resolution OGCM configurations will produce rather diffusive boundary currents. For the Atlantic, the Gulf Stream system is a classical example of this problem (e.g. Bleck et al., 1995), but also the OW and the DWBCs will be degraded in model systems applying grid spacing comparable to or larger than the characteristic spatial scales of the currents.

Numerical diffusion associated with the advection and diffusion terms in the prognostic transport equations will also have a diffusive effect on the boundary currents. In contrast to conventional coordinate OGCMs (like the fixed level or z-coordinate models), there is essentially no false diapycnal mixing in the isopycnic coordinate model used in this study. Also the numerical mixing associated with the Smolarkiewicz and Clark (1986) flux corrected transport scheme is fairly weak (this is illustrated by the clear difference in the isopycnal spreading of CFC-11 between Exps. 2 and 3, see Figs. 11c and 11d). In general, numerical schemes with limited numerical smoothing (e.g. Drange and Bleck, 1997) need to be used in OGCM simulations like those presented here.

Further complications are linked to the fact that mixing across surfaces of constant density (or neutral surfaces) are generated by a variety of processes, including mixing caused by dissipation of energy from internal waves in the open ocean, mixing against topography and mixing generated by (surface, internal or near sea bed) shear flows. The N^{-1}-dependent diapycnal mixing used in this study is simple, but is still

more elaborate than fixed values used in many present-day climate OGCMs (see for instance discussion in Nilsson and Walin, 2001). A more complete description of the diapycnal mixing would include parameterizations of the above mentioned processes, which is beyond the scope of this paper.

Finally, the natural variability of the mixing in the sup-polar region is particularly important to the ventilation of the deep North Atlantic Ocean, and this variability contributes significantly to the variability of the MOC (Curry and McCartney, 2001). A consequence of the applied climatological monthly mean atmospheric forcing fields is a fairly constant MOC in the simulations presented here (Fig. 4). In reality, year-to-year variability in the forcing, possibly in combination of internal ocean circulation modes (Bentsen, 2002), leads to significant variations in the MOC. Therefore, a model system like the system presented here should also be validated based on the use of synoptic (i.e., daily) atmospheric forcing fields. Such integrations are ongoing, and will be presented elsewhere.

It is concluded that the presented simulations provide detailed insight into the effect the isopycnal and diapycnal diffusion parameterizations have on surface to abyss ventilation, dispersive mixing and advective spreading on some of the key water masses in the North Atlantic. It is encouraging that the simulated distribution of the CFCs in Exp. 3 are as close to the observed distributions as is the case. Furthermore, the major model deficiencies (i.e., too sluggish DWBCs) are believed to be linked to an intricate interplay between the fairly coarse model resolution, the use of monthly mean climatological forcing and possibly unresolved mixing processes in the model. Therefore, continuous improvements and refinements of this and similar model systems are required to improve the model performance further. Irrespective of the detected problems, the CFC study shows promising prospects for simulating multi-annual to dedacal scale variability of the present-day climate system, and thereby also for assessing possible changes in the variability of the marine climate system as the human-induced global warming continues.

5. Acknowledgments

This study has been supported by the G. C. Rieber Foundations, Norsk Hydro as, the Norwegian Research Council through the RegClim and the Programme of Supercomputing projects, and the projects GOSAC (EVK2-2000-00080) and TRACTOR (ENV4-CT97-0495) under the EC Environment and Climate Programme. We are grateful to Drs. W. M. Smethie, R. F. Weiss, P. Salameh and G. Parrilla for providing CFC data from the cruises used in the study. One anonymous reviewer and Patric Monfray's review greatly improved the manuscript. This is contribution no. A0014 from the Bjerknes Centre for Climate Research.

REFERENCES

Andrie, C., Ternon, J., Bourles, B., Gouriou, Y. and Oudot, C. 1999. Tracer distributions and deep circulation in the western tropical Atlantic during CITHER 1 and ETAMBOT cruises, 1993–1996. *J. Geophys. Res.* **104**, C9, 21 195–21 215.

Arakawa, A. and Lamb, V. 1977. Computational design of the basic processes of the UCLA General Circulation Model. *Meth. Comput. Phys.* **17**, 174–265.

Bentsen, M., Evensen, G., Drange, H. and Jenkins, A. D. 1999. Coordinate transformation on a sphere using conformal mapping. *Mon. Wea. Rev.* **127**, 2733–2740.

Bentsen, M. and Drange, H. 2000. *Parameterizing surface fluxes in ocean models using the NCEP/NCAR reanalysis data*. Tech. Rep. No. 4. Kjeller, Norway: Norwegian Institute for Air Research. (In *RegClim, Regional Climate Development Under Global Warming* General Technical Report)

Bentsen, M. 2002. *Modelling ocean climate variability of the North Atlantic and the Nordic Seas,*. Doctoral dissertation, University of Bergen, Bergen, Norway.

Bleck, R., Rooth, C., Hu, D. and Smith, L. T. 1992. Salinity-driven thermohaline transients in a wind- and thermohaline-forced isopycnic coordinate model of the North Atlantic. *J. Phys. Oceanogr.* **22**, 1486–1515.

Bleck, R., Dean, S., Keefe, M. O. and Sawdey, A. 1995. A comparison of data-parallel and message-passing versions of the Miami Isopycnic Coordinate Ocean Model. *Parallel Computing* **21**, 1695–1720.

Bower, A. and Hunt, H. 2000. Lagrangian observations of deep western boundary current in the north atlantic ocean. Part i: Large-scale pathways and spreading rates. *J. Phys. Oceanogr.* **30**, 764–783.

Broecker, W. 1991. The great ocean conveyor. *Oceanography* **4**, 79–89.

Bryan, F. 1987. Parameter sensitivity of primitive equation ocean general circulation models. *J. Phys. Oceanogr.* **17**, 970–985.

Bryden, H., Griffiths, M., Lavin, A., Millard, R., Parrilla, G. and Smethie, W. 1996. Decadal changes in water mass

characteristics at 24°N in the subtropical North Atlantic Ocean. *J.Climate* **9**, 3162–3186.

Curry, R. and McCartney, M. S. 2001. Ocean gyre circulation changes associated with the North Atlantic Oscillation. *J. Phys. Oceanogr.* **31**, 3374–3400.

Dickson, R. R. and Brown, J. 1994. The production of North Atlantic Deep Water: Sources, rates and pathways. *J. Geophys. Res.* **99**, C6, 12 319–12 341.

Dixon, K., Bullister, J., Gammon, R. and Stouffer, R. 1996. Examining a coupled climate model using CFC-11 as an ocean tracer. *Geophys. Res. Lett.* **23**, 1957–1960.

Drange, H. and Simonsen, K. 1996. *Formulation of air–sea fluxes in the ESOP2 version of MICOM*Tech. Rep. No. 125. Edv. Griegsv. 3A, N-5059 Solheimsviken, Norway: Nansen Environmental and Remote Sensing Center.

Drange, H. and Bleck, R. 1997. Multi-dimensional forward-in-time and upstream-in-space based differencing for fluids. *Mon. Wea. Rev.* **125**, 616–630.

Dutay, J., Bullister, J., Doney, S., Orr, J., Najjar, R., Caldeira, K., Campin, J., Drange, H., Follows, M., Gao, Y., Gruber, N., Hecht, M., Ishida, A., Joos, F., Lindsay, K., Madec, G., Marier-Reimer, E., Marshall, J., Matear, R., Monfray, P., Plattner, G., Sarmiento, J., Schlitzer, R., Slater, R., Totterdell, I., Weirig, M., Yamanaka, Y. and Yool, A. 2002. Evaluation of ocean model ventilation with CFC-11: comparison of 13 global ocean models. *Ocean Modelling* **4**, 89–120.

Eden, C. and Jung, T. 2001. North Atlantic interdecadal variability: oceanic response to the North Atlantic Oscillation. *J. Climate* **14**, 676–691.

England, M. and Holloway, G. 1998. Simulations of CFC content and water mass age in the deep North Atlantic. *J. Geophys. Res.* **103**, C8, 15 885–15 901.

England, M. and Maier-Reimer, E. 2001. Using chemical tracers to assess ocean models. *Rev. Geophys.* **39**, 29–70.

Fairall, C. W., Bradley, E. F., Rogers, D. P., Edson, J. B. and Young, G. S. 1996. Bulk parameterization of air–sea fluxes for Tropical Ocean-Global Atmosphere Coupled-Ocean Atmosphere Response Experiment. *J. Geophys. Res.* **101**, C2, 3747–3764.

Friedrich, H. and Levitus, S. 1972. An approximation to the equation of state for sea water, suitable for numerical ocean models. *J. Phys. Oceanogr.* **2**, 514–517.

Furevik, T., Bentsen, M., Drange, H., Johannessen, J. A. and Korablev, A. 2002. Temporal and spatial variability of the sea surface salinity in the Nordic Seas. *J. Geophys. Res.* **107**, C12, 10-1–10-16.

Ganachaud, A. and Wunsch, C. 2000. Improved estimates of global ocean circulation, heat transport and mixing from hydrographic data. *Nature* **408**, 453–457.

Gargett, A. 1984. Vertical eddy in the ocean interior. *J. Marine. Res.* **42**, 359–393.

Gaspar, P. 1988. Modeling the seasonal cycle of the upper ocean. *J. Phys. Oceanogr.* **18**, 161–180.

Gloersen, P., Campbell, W. J., Cavalieri, D. J., Comiso, J. C. and Zwally, C. L. P. H. J. 1992. *Artic and Antarctic sea ice, 1978–1987*. National Aeronautics and Space Administration, Washington, D.C., USA.

Gordon, A. 1986. Interocean exchange of thermocline water. *J. Geophys. Res.* **91**, 5037–5046.

Hansen, B. and Østerhus, S. 2000. North Atlantic–Nordic Seas exchanges. *Prog. Oceanogr.* **45**, 109–208.

Harder, M. 1996. *Dynamik, Rauhigkeit und Alter des Meereises in der Arktis*. Unpublished doctoral dissertation, Alfred-Wegner-Institut für Polar- ind Meeresforschung, Bremerhaven, Germany.

Hartman, D. L. 1994. *Global physical climatorology*. Academic Press, New York, 171–203.

Hasumi, H. and Suginohara, N. 1999. Effects of locally enhanced vertical diffusivity over rough bathymetry on the world ocean circulation. *J. Geophys. Res.* **104**, C10, 23 367–23 374.

Hibler, W. 1979. A dynamic thermodynamic sea ice model. *J. Phys. Oceanogr.* **9**, 815–846.

Jones, E., Rudels, B. and Anderson, L. 1995. Deep waters of the Arctic Ocean: origins and circulation. *Deep Sea Res.* **42**, 737–760.

Kalnay, E., et al. 1996. The NCEP/NCAR 40-Year Reanalysis Project. *Bull. Amer. Meteorol. Soc.* **77**, 437–471.

Ledwell, J. R. and Watson, A. J. 1993. Evidence for slow mixing across the pycnocline from an open ocean tracer-release experiment. *Nature* **364**, 701–703.

Ledwell, J. R., Watson, A. J. and Law, C. S. 1998. Mixing of a tracer in the pycnocline. *J. Geophys. Res.* **103**, C10, 21 449–21 529.

Ledwell, J. R., Montgomery, E., Polzin, K., Laurent, L., Schmitt, R. and Toole, J. 2000. Evidence for enhanced mixing over rough topography in the abyssal ocean. *Nature* **403**, 179–182.

Levitus, S. and Boyer, T. P. 1994. *World Ocean Atlas 1994, Volume 4: Temperature*. NOAA Atlas NESDIS 4. Washington, D.C., USA.

Levitus, S., Burgett, R. and Boyer, T. P. 1994. *World Ocean Atlas 1994, Volume 3: Salinity,*. NOAA Atlas NESDIS 3. Washington, D.C., USA.

Manabe, S. and Stouffer, R. 1999. The role of thermohaline circulation in climate. *Tellus* **51B**, 92–109.

McCartney, M. S. and Talley, L. D. 1982. The subpolar mode water of the North Atlantic Ocean. *J. Phys. Oceanogr.* **12**, 1169–1188.

McDougall, T. and Dewar, W. 1998. Vertical mixing, cabbeling and thermobaricity in layered models. *J. Phys. Oceanogr.* 1458–1480.

Munk, W. and Wunsch, C. 1998. Abyssal recipes ii: Energetics of tidal and wind mixing. *Deep Sea Res.* **45**, 1977–2010.

New, A., Bleck, R., Jia, Y., Marsh, R., Huddleston, M. and Bernard, S. 1995. An ispoycnic model study of the North Atlantic. Part I: Model experiment. *J. Phys. Oceanogr.* **25**, 2679–2711.

Nilsson, J. and Walin, G. 2001. Freshwater forcing as a booster of thermohaline circulation. *Tellus* **53A**, 628–640.

Pickart, R. 1992. Water mass components of North Atlantic deep western boundary current. *Deep Sea Res., Part A* **39**, 1553–1572.

Pickart, R., Smethie W., Jr, Lazier, J., Jones, E. and Jenkins, W. 1996. Eddies of newly formed upper Labrador Sea Water. *J. Geophys. Res.* **101**, 20 711–20 726.

Rahmstorf, S. and Ganopolski, A. 1999. Long-term global warming scenarios computed with an efficient coupled climate model. *Clim. Change* **43**, 353–367.

Roach, A., Aagaard, K., Pease, C., Salo, S., Weingartner, T., Pavlov, V. and Kulakov, M. 1995. Direct measurements of transport and water properties through the Bering Strait. *J. Geophys. Res.* **100**, 18 443–18 457.

Rudels, B., Jones, E., Anderson, L. and Kattner, G. 1994. On the intermediate depth waters of the Arctic Ocean. In *The Polar Oceans and Their Role in Shaping the Global Environment: The Nansen Centennial Volume*(eds. O. Johannessen, R. Muench and J. Overland)(Vol. 85, of AGU Geophysical Monograph, 33–46). American Geophysical Union, Washington, D.C.

Schmittner, A. and Weaver, A. 2001. Dependence of multiple climate states on ocean mixing parameters. *Geophys. Res. Lett.* **28**, 1027–1030.

Schmitz Jr. W. J. 1995. On the interbasin-scale thermohaline circulation. *Rev. Geophys.* **33**, 151–173.

Smethie, Jr, W. M., Fine, R., Putzka, A. and Jones, E. 2000. Tracing the flow of north atlantic deep water using chlorofluorocarbons. *J. Geophys. Res.* **105**, C6, 14 297–14 323.

Smolarkiewicz, P. K. 1984. A fully multidimensional positive definite advection transport algorithm with small implicit diffusion. *J. Comput. Phys.* **54**, 325–362.

Smolarkiewicz, P. K. and Clark, T. L. 1986. The multidimensional positive definite advection transport algorithm: Further development and applications. *J. Comput. Phys.* **67**, 396–438.

Sun, S. and Bleck, R. 2001. Thermohaline circulation studies with an isopycnic coordinate ocean model. *J. Phys. Oceanogr.* **31**, 2761–2782.

Toole, J. M., Polzin, K. L. and Schmitt, R. W. 1994. Estimates of diapycnal mixing in the abyssal ocean. *Science* **264**, 1120–1123.

Walker, S., Weiss, R. and Salameh, P. 2000. Reconstructed histories of the annual mean atmospheric mole fractions for halocarbons CFC-11, CFC-12, CFC-113, and carbon tetrachloride. *J. Geophys. Res.* **105**, C6, 14 285–14 296.

Wanninkhof, R. 1992. Relationship Between Wind Speed and Gas Exchange Over the Ocean. *J. Geophys. Res.* **97**, C5, 7373–7382.

Warren, B. 1981. Deep circulation of the world ocean. In: *Evolution of Physical Oceanography, Scientific Surveys in Honor of Henry Stommel*. (eds. B. A. Warren and C. Wunsch), MIT Press, New York, 6–41.

Weiss, R. F., Bullister, J. L., Gammon, R. H. and Warner, M. J. 1985. Atmospheric chlorofluoromethanes in the deep equatorial Atlantic. *Nature* **314**, 608–610.